The Cryosphere Discuss., https://doi.org/10.5194/tc-2017-123
Manuscript under review for journal The Cryosphere
Discussion started: 18 July 2017

The Cryosphere Discussions
Open Access
EGU

Snowmelt response to simulated warming across a large elevation gradient, southern Sierra Nevada, California

Keith N. Musselman[1], Noah P. Molotch[2], and Steven A. Margulis[3]

[1]National Center for Atmospheric Research, Boulder, Colorado, USA

[2]Department of Geography, Institute of Arctic and Alpine Research, University of Colorado, Boulder, USA & Jet Propulsion Laboratory, California Institute of Technology, Pasadena, USA

[3]Department of Civil and Environmental Engineering, University of California, Los Angeles, California, USA

Correspondence to: Keith N. Musselman (kmussel@ucar.edu)

The Cryosphere Discuss., https://doi.org/10.5194/tc-2017-123
Manuscript under review for journal The Cryosphere
Discussion started: 18 July 2017

The Cryosphere Discussions
Open Access
EGU

10 **Abstract**

11 In a warmer climate, the fraction of annual meltwater produced at high melt rates is projected to
12 decline due to a contraction of the melt season to an earlier period of lower energy. How
13 snowmelt rates, including extreme events relevant to flood risk, may respond to a range of
14 warming over a mountain front remains poorly known. We present a model sensitivity study of
15 snowmelt response to warming across a 3600 m elevation gradient in the southern Sierra
16 Nevada, USA. A snow model was run for three distinct years and verified against extensive
17 ground observations. To simulate the impact of climate warming on meltwater production,
18 measured meteorological conditions were modified by +1°C to +6°C. The total annual snow
19 water volume exhibited linear reductions (-10% $°C^{-1}$) consistent with previous studies. However,
20 the sensitivity of snowmelt rates to successive degrees of warming varied nonlinearly with
21 elevation. Middle elevations and years with more snowfall were prone to the largest reductions
22 in snowmelt rates, with lesser changes simulated at higher elevations. Importantly, simulated
23 warming causes extreme daily snowmelt (99^{th} percentiles) to increase in spatial extent and
24 intensity and shift from spring to winter. The results offer critical insight into the sensitivity of
25 mountain snow water resources and how the rate and timing of water availability may change in
26 a warmer climate. The identification of future climate conditions that may increase extreme melt
27 events is needed to address the climate resilience of regional flood control systems.

The Cryosphere Discuss., https://doi.org/10.5194/tc-2017-123
Manuscript under review for journal The Cryosphere
Discussion started: 18 July 2017

1. Introduction

Seasonal snow accumulation and melt in mountainous areas are critical components of the regional hydrologic cycle with important controls on climate, ecosystem function, flood risk, and water resources [*Bales et al.*, 2006; *Barnett et al.*, 2005]. Warmer temperatures are expected to reduce snowpack volume and persistence [*Gleick*, 1987; *Knowles and Cayan*, 2004; *Mote et al.*, 2005] by shifting precipitation from snowfall to rain [*Knowles et al.*, 2006] and causing earlier snowmelt [*Stewart et al.*, 2004]. Studies of historical observations in the western U.S. have identified recent declines in spring snowpack [*Mote et al.*, 2005], diminished snowmelt runoff volumes [*Dettinger and Cayan*, 1995; *McCabe and Clark*, 2005] and earlier spring runoff [*Stewart et al.*, 2004]. Most of these studies have attributed the observed trends to anomalously warm spring and summer temperatures of recent decades. *Fyfe et al.* [2017] report that the recent snowpack declines are not replicable with climate model simulations forced by natural changes (i.e., internal variability) alone, but are resolved when both natural and anthropogenic changes are considered.

Continued warming is expected. General Circulation Models (GCMs) project increases in global average temperatures ranging from 0.7°C ± 0.4°C to 6.5°C ± 2.0°C for the lowest and highest greenhouse gas emission scenarios, respectively, for the end of the next century [*Stocker et al.*, 2013]. The effects of a warmer climate on the snow-dominated hydrology of the Sierra Nevada are generally recognized to include higher winter storm runoff and flood risk, and reduced summer low-flows [*Dettinger*, 2011; *Dettinger et al.*, 2004; *Godsey et al.*, 2013; *Knowles and Cayan*, 2002; *Lettenmaier and Gan*, 1990]. It is not well understood how present-day snowmelt rates may respond to the range of projected warmer temperature scenarios and, particularly, how those changes will impact water availability over large elevation gradients.

The Cryosphere Discuss., https://doi.org/10.5194/tc-2017-123
Manuscript under review for journal The Cryosphere
Discussion started: 18 July 2017

Elevation is a dominant explanatory variable of mountain snow-cover persistence [*Girotto et al.*, 2014b], ranking in importance above solar radiation and terrain aspect for many basins in the western U.S. [*Molotch and Meromy*, 2014]. Snowpack response to warmer temperatures exhibits strong nonlinear elevation dependencies [*Brown and Mote*, 2009; *Knowles and Cayan*, 2004]. For example, slight warming can cause drastic hydrologic response at lower elevations as rain becomes the predominant hydrologic input and snow-cover becomes seasonally intermittent or negligible [*Hunsaker et al.*, 2012; *Marty et al.*, 2017; *Nolin and Daly*, 2006]. At higher and cooler elevations, snowmelt may remain a substantial component of the annual hydrologic input in a warmer climate, but the timing and rate of melt is altered. Rapid and prolonged spring snowmelt is unique to these mountain environments [*Trujillo and Molotch*, 2014]. This efficient runoff generation mechanism [*Barnhart et al.*, 2016] produces water resources of vast economic importance [*Sturm et al.*, 2017]. Improved understanding of regional elevation-dependent snowmelt response to warming is a key step toward better predicting and interpreting model estimates of basin-wide runoff.

In a warmer climate, the fraction of meltwater produced at high melt rates is projected to decrease due to a contraction of the historical melt season to a period of lower available energy [*Musselman et al.*, 2017]. Because streamflow is a nonlinear response to hydrologic input, slight reductions in snowmelt rates may disproportionately reduce runoff. Despite recent advances in process understanding, the sensitivity of snowmelt rates to a range of potential warming over a foothills-to-headwaters elevation profile remains poorly known. The topic is a key determinant of changes in how precipitation is partitioned among soil storage, evapotranspiration, and runoff with implications on ecological response [*Tague and Peng*, 2013; *Trujillo et al.*, 2012] and regional water resources [*Gleick and Chalecki*, 1999; *Vano et al.*, 2014].

The Cryosphere Discuss., https://doi.org/10.5194/tc-2017-123
Manuscript under review for journal The Cryosphere
Discussion started: 18 July 2017

We present a climate sensitivity experiment to investigate how carefully-verified model simulations of historical snow water equivalent (SWE) and melt rates respond to successively warmer temperatures that span the range of projected wintertime warming over western North America for this century [*Van Oldenborgh et al.*, 2013]. A controlled experiment with a physically based snow model promotes a detailed analysis of the following research questions: 1) How do SWE and snowmelt rates vary with elevation and how do those gradients vary amongst dry, average, and wet snow seasons? and 2) How do historical SWE and snowmelt rates respond to successive degrees of warming?

2. Methods

To evaluate the response of SWE and snowmelt dynamics to warmer temperatures, we conduct a reanalysis of historical snow seasons using the physically based Alpine3D [*Lehning et al.*, 2006] snow model run at 100 m grid spacing over a mountainous region spanning a 3600-m elevation gradient in the southern Sierra Nevada, California. Snowpack simulations for three historical snow seasons were first verified against multi-scale, ground-based observations. Simulated snowpack characteristics over discrete elevation bands were then examined for their sensitivity to warmer conditions using a delta-change approach in which observed air temperature values and the longwave radiative equivalent were augmented by +1°C to +6°C in +1°C increments. Given the relatively small (< 10%) precipitation changes projected for central and southern California [*Cayan et al.*, 2008], and a lack of agreement of climate models on the sign of projected precipitation changes [*Seager et al.*, 2013], the focus of the current study is on the snowpack response to simulated warming rather than combined changes in temperature and precipitation. Sensitivity was examined for three historical snow years representative of the

96 climatological range in snowfall (years with below-average, average, and above-average
97 snowfall), snow-cover duration, and precipitation timing. The following sub-sections describe
98 the details of our model experiment, verification, and analysis methods.

99 **2.1. Study domain**

100 The study was conducted over a 1648 km^2 area encompassing the 1085 km^2 Kaweah River basin
101 on the western slope of the southern Sierra Nevada, California, USA (36.4ºN, 118.6ºW) (Fig. 1).
102 The elevation of the Kaweah River basin ranges from 250 m to over 3800 m asl. The land-cover
103 and climate of the domain vary substantially over the full 3633 m elevation range (Fig. 1).
104 Approximately 98% of the domain is comprised of four land-cover types [*Fry et al.*, 2011]:
105 conifer forest (58%), shrub (26%), bare soil / rock (10%), and grass / tundra (4%) (Fig. 1). A mix
106 of grassland, shrub, and oak woodlands characterizes the vegetation of the low elevation foothills
107 (< 1600 m asl), where mild and wet winters and arid summers characterize the climate and a 660
108 mm average annual precipitation is rain-dominated [*NPS*, 2017]. At middle elevations (1600 m
109 to 3000 m asl), mixed conifer forest stands are dominant, including some of the world's only
110 giant sequoia (*Sequoiadendron giganteum*) groves. The middle elevation climate is cool with
111 seasonally snow-covered winters and warm, dry summers, and the average annual precipitation
112 exceeds 1080 mm [*NPS*, 2017]. Forest vegetation of the sub-alpine zone, between 3000 m and
113 3500 m asl, is sparse and coniferous. Precipitation is not measured at these upper elevations. At
114 the highest elevations (> 3500 m asl), the land cover is bedrock with sparse alpine vegetation and
115 snow-cover typically persists from November to July.

116 The domain includes two research basins: the 7.22 km^2 forested Wolverton basin and the
117 19.1 km^2 largely alpine Tokopah basin (Fig. 1). The Wolverton basin is representative of

The Cryosphere Discuss., https://doi.org/10.5194/tc-2017-123
Manuscript under review for journal The Cryosphere
Discussion started: 18 July 2017

118 regional forested mid-elevations. A detailed description of the Wolverton basin instrumentation
119 is provided in *Musselman et al.* [2012a]. The 19.1 km^2 Tokopah basin is representative of small
120 headwater basins in the southern Sierra Nevada [*Tonnessen*, 1991]. It is instrumented with
121 numerous meteorological stations and has been the subject of many studies on snow distribution
122 [*Elder et al.*, 1988; *Girotto et al.*, 2014a; *Jepsen et al.*, 2012; *Marks et al.*, 1992; *Molotch et al.*,
123 2005] and biogeochemistry [*Perrot et al.*, 2014; *Sickman et al.*, 2003; *Williams and Melack*,
124 1991]. We use ground-based observations from these research basins to verify the model as
125 described in Sect. 2.4.

126 **2.2. Snow model**

127 Alpine3D [*Lehning et al.*, 2006] is a land surface model with an emphasis on snow
128 process representation. It has been used in previous snow process studies [*Bavay et al.*, 2009;
129 *Magnusson et al.*, 2011; *Michlmayr et al.*, 2008; *Mott et al.*, 2008] and projections of future snow
130 or runoff [e.g. *Bavay et al.*, 2013; *Bavay et al.*, 2009; *Kobierska et al.*, 2013; *Kobierska et al.*,
131 2011; *Marty et al.*, 2017]. At the core of Alpine3D is the one-dimensional SNOWPACK model
132 [*Bartelt and Lehning*, 2002], which has been validated in alpine [e.g. *Etchevers et al.*, 2004] and
133 forested [e.g. *Rutter et al.*, 2009] environments, including a previous study in the Wolverton
134 basin using a subset of the forcing and verification data presented herein [*Musselman et al.*,
135 2012b]. At each model grid cell, mass and energy balance equations for vegetation, snow, and
136 soil columns are solved with external forcing provided by the atmospheric variables described in
137 Sect. 2.3.

138 The bottom (soil) boundary conditions were treated with a constant geothermal heat flux
139 of 0.06 W m^{-2} applied at the base of a six-layer soil module [see *Musselman et al.*, 2012b for

more information]. In the case of vegetation cover, the surface-atmosphere boundary conditions were solved for in a single-layer canopy module [see *Musselman et al.*, 2012b]. Wind transport of snow is not considered in this model implementation. The SNOWPACK model treats the snowpack as an arbitrary number of layers. New-snow density and snow albedo parameterizations used in previous studies in the European Alps [*Bavay et al.*, 2013] were found to work well in the Wolverton basin [*Musselman et al.*, 2012b] and are used in the current study. Other land-cover parameters such as canopy height and leaf area index were specified according to land-cover classifications discussed in Sect. 2.3. A simple 1.2°C air temperature threshold was used to distinguish rain from snow, slightly higher than the 1.0°C value used in *Musselman et al.* [2012b].

2.3. Model input data

2.3.1. Topography and land-cover data

The elevation and land-cover across the domain were represented at 100 m grid spacing. Land-cover classification (Fig. 1) was specified from the National Land Cover Database (NLCD) [*Fry et al.*, 2011]. In addition to the land-cover classes listed in Fig. 1, forest-covered grid cells were aggregated into coniferous, mixed, and deciduous categories based on the dominant species within each cell. The NLCD canopy density values, used to parameterize canopy snow interception and snow surface energy fluxes, were binned from 5% to 85% in 10% intervals. Grid elements containing vegetation were specified to have an effective leaf area index and canopy height, respectively, of 0.5 m^2 m^{-2} and 1.5 m for shrub/chaparral, 1.2 m^2 m^{-2} and 20 m for deciduous, 2.0 m^2 m^{-2} and 30 m for mixed, and 2.7 m^2 m^{-2} and 40 m for coniferous forests.

The Cryosphere Discuss., https://doi.org/10.5194/tc-2017-123
Manuscript under review for journal The Cryosphere
Discussion started: 18 July 2017

161 **2.3.2 Meteorological data**

162 Hourly meteorological observations were available from 19 stations within the domain (Fig. 1
163 and Table 1). Sixteen stations recorded hourly air temperature and six reported precipitation
164 (Table 1). The Ash Mountain station at 527 m asl provided the only low elevation precipitation
165 measurements. The Lower Kaweah station, and the Atwell, Giant Forest, and Bear Trap Meadow
166 stations are located within a narrow elevation band of 1926 to 2073 m asl (Fig. 1 and Table 1).
167 Data from a single higher station (Hockett Meadow; 2592 m asl) were not used because of gauge
168 error for the time period of interest. Precipitation gauge catch efficiency was specified as 0.95 for
169 rain and 0.6 for snow, using the 1.2°C air temperature threshold as a determinant of precipitation
170 phase. Incoming shortwave radiation was provided from the Topaz Lake meteorological station
171 (Fig. 1; Table 1). The direct beam was adjusted for grid cell-specific terrain shading and
172 elevation dependency and the diffuse component was assumed spatially uniform for each time
173 step [see *Bavay et al.*, 2013 for details]. The shortwave radiation data are well-correlated with
174 measurements at middle elevations [*Musselman et al.*, 2012a] and are used to model the full
175 domain.

176 The remaining meteorological variables required spatial interpolation from station
177 locations to all grid cells. Because elevation can have a profound influence on many of the
178 meteorological variables, several of the interpolation methods used linear elevation trends.
179 Interpolations were conducted with the data access and pre-processing library MeteoIO [*Bavay*
180 *and Egger*, 2014] and computed with an Inverse Distance Weighting (IDW) algorithm with
181 elevation lapse rate adjustments for air temperature, wind speed, and precipitation. Lapse rates
182 were computed for each hourly time step using a regression technique [*Bavay and Egger*, 2014]
183 applied to observations from all available stations. If the correlation coefficient was less than 0.6,

184 then a constant elevation lapse rate of -0.008 °C m^{-1} was used for air temperature and a
185 standardized elevation trend of 0.0006 m^{-1} was used for precipitation. The incoming longwave
186 radiation measured at the Topaz Lake station was distributed to all grid cells with a constant
187 elevation lapse rate of -0.03125 W m^{-2} m^{-1} as in *Bavay et al.* [2013]. Relative humidity was
188 interpolated as in *Liston and Elder* [2006].

189 **2.4. Snow observations and validation data**

190 **2.4.1 Seasonal basin-scale snow surveys**

191 Snow surveys were conducted in the two research basins for three snow seasons: 2008, 2009,
192 and 2010. Three snow surveys of the forested Wolverton basin were conducted each in 2008 and
193 2009. The survey timing coincided with periods of accumulation (mid-February), maximum
194 accumulation (mid-March), and melt (late-April). In all three years, early-April surveys of the
195 alpine Tokopah basin were conducted. In 2009, two additional Tokopah basin surveys captured
196 accumulation (early-March) and melt (mid-May). Surveys were conducted with graduated
197 probes to measure snow depth at waypoint locations on a 250 m grid. Surveyors navigated to the
198 waypoints using Geographic Position System units. At each waypoint, three snow depth
199 measurements separated by five meters were made along a north-south axis. In total over the
200 three years, 1,494 waypoints were surveyed. During each survey, snow density was recorded
201 from snow pits conducted at lower and upper elevations to capture the basin range of snow
202 density; only one snow pit was dug during the 2010 Tokopah survey. An undisturbed snow face
203 was excavated to ground and snow density in duplicate columns was measured in 10 cm vertical
204 intervals by weighing snow samples acquired with a 1000 cm^3 cutter. In total, 26 snow pits were
205 measured over the three years. The average snow density at all pits made during a survey was
206 used to estimate SWE at waypoint locations, which represent the average of three depth

The Cryosphere Discuss., https://doi.org/10.5194/tc-2017-123
Manuscript under review for journal The Cryosphere
Discussion started: 18 July 2017

measurements. This approach assumes that basin-scale snow density varies less than snow depth [*López-Moreno et al.*, 2013].

Simulated SWE at model grid-elements containing waypoint positions are evaluated against the snow survey values. Three model evaluation metrics are reported. The model bias is computed as the average difference ('modeled minus measured') of n survey measurements for each waypoint measurement SWE_{o_i} and corresponding model grid cell SWE_{m_i}. The root-mean-square error (RMSE) is computed as

$$\mathrm{RMSE} = \sqrt{\frac{1}{n}\sum_{i=1}^{n}\left(SWE_{m_i} - SWE_{o_i}\right)^2} \qquad \text{Eq. (1)}$$

and the normalized mean square error (NMSE) value is computed as

$$\mathrm{NMSE} = \frac{\overline{(SWE_m - SWE_o)^2}}{\overline{SWE_m}\;\overline{SWE_o}} \qquad \text{Eq. (2)}$$

where the overbars denote the mean over all waypoint locations. The NMSE metric facilitates model performance comparisons amongst basins, months, and years.

2.4.2 Monthly plot-scale snow surveys

Monthly (1 February – 1 May) manual SWE measurements in the Sierra Nevada are made by the California Cooperative Snow Survey (CCSS) program to monitor regional water resources. Seven snow course sites are located within the study domain (Table 1); the sites range in elevation from 1951 m to 2942 m. At each snow course, linear transects of approximately 10 SWE measurements made with Federal snow tube samplers are averaged to represent the mean SWE over a distance similar to the 100 m grid cell spacing. The survey measurements thus provide a SWE estimate that is arguably more representative of the average value within a

227 corresponding model grid cell than the three point-measurements of the basin-scale surveys or a
228 single automated SWE station measurement. Modeled SWE values for each survey date at the
229 grid cells corresponding to each snow course location were evaluated against measured values.

230 **2.4.3 Automated snow depth sensor network**

231 In addition to the repeated basin- and plot-scale manual snow surveys, the Wolverton basin
232 includes a network of 24 ultrasonic snow depth sensors. Four research sites at different
233 elevations (2253 m, 2300 m, 2620 m, and 2665 m asl) each includes six snow depth sensors and
234 each site falls within a different 100 m x 100 m model grid cell. The range of snow depth
235 measured at the six sensors provides a robust estimate of the snow depth, and thus model skill, at
236 four grid cells spanning slope, aspect, forest density, and elevation in the basin.

237 **2.4.4 Automated SWE stations**

238 Daily SWE observations were available from three CCSS automated stations (i.e., snow
239 'pillows') at middle elevations: Giant Forest (1951 m asl), Big Meadows (2317 m asl), and
240 Farewell Gap (2896 m) (Table 1 and Fig. 1). Modeled SWE fields were evaluated against these
241 station observations. The climatological mean SWE record (26 years at Giant Forest and Big
242 Meadows; 15 years at Farewell Gap) was used to evaluate how the three snow seasons studied
243 here compare to the long-term average.

244 **2.5. Experimental design**

245 The model was run to simulate seasonal snow dynamics for three reference water years (1
246 October, 2007 – 30 September, 2010) for which the extensive ground-based observations were
247 available. Model estimates of snow depth and SWE were evaluated against the observations.

The Cryosphere Discuss., https://doi.org/10.5194/tc-2017-123
Manuscript under review for journal The Cryosphere
Discussion started: 18 July 2017

Six warmer temperature scenarios for each of the three reference years were simulated by increasing the hourly measured air temperature from the 19 regional meteorological stations by +1°C to +6°C in 1°C increments. The lower (+1°C) and upper (+6°C) limits of simulated warming correspond to the average winter air temperature increases projected for the year 2100 in western North America in the Representative Concentration Pathway (RCP) emissions scenarios 2.6 (lowest emissions) and 8.5 (highest emissions), respectively [see top-right panel in Fig. A1.16 in *Van Oldenborgh et al.*, 2013]. For each warmer temperature scenario ($+n$°C) and hourly time step *t*, the incoming longwave radiation $LW_{\downarrow t}$ [W m^2] measured at the Topaz Lake station was adjusted for the increase in effective radiative temperature resulting from the warmer air. The *in-situ* atmospheric emissivity ϵ_t was estimated from the hourly air temperature T_{a_t} [°C]:

$$\epsilon_t = \frac{LW_{\downarrow t}}{\sigma(T_{a_t}+273.15)^4} \quad \text{Eq. (3)}$$

where σ is the Stefan-Boltzmann constant (5.670373x10^{-8} W m^{-2} K^{-4}). The longwave radiation was adjusted for an effective radiative temperature increase of *n* [°C] as:

$$LW_{\downarrow t_{(T_a+n)}} = \epsilon_t \sigma (T_{a_t} + 273.15 + n)^4 \quad \text{Eq. (4)}$$

Relative humidity was held constant to allow water vapor pressure to vary in a manner consistent with the ideal gas law [*Rasouli et al.*, 2015]. A lack of clear projected wintertime precipitation response to climate change in the southern Sierra Nevada [see Fig. A1.18 in *Van Oldenborgh et al.*, 2013] prompted our focus on temperature sensitivity rather than a combination of temperature and precipitation. Observed and adjusted meteorological variables representative of the warmer scenarios were interpolated to domain grid cells as described in Sect. 2.3.2. The model was run as in the reference scenarios (Sect. 2.2).

The Cryosphere Discuss., https://doi.org/10.5194/tc-2017-123
Manuscript under review for journal The Cryosphere
Discussion started: 18 July 2017

Daily maps of simulated SWE, snow depth, and sublimation were output for each of the three reference years and six temperature perturbations (21 simulations). For each simulation, we evaluate the elevational distribution of SWE (mm), daily melt (mm day^{-1}), and total annual melt reported as the depth per unit area (mm per 100 m grid cell) and the total volume (km^3). The daily depletion of SWE, less the daily atmospheric exchange with the snow surface (i.e., sublimation and accretion of ice), is a first-order estimate of daily snowmelt (hereafter, snowmelt rate). The total annual meltwater is then the annual sum of daily snowmelt.

To evaluate how SWE and melt in each scenario varied with elevation, metrics were averaged or summed into 200 elevation bands, each encompassing ~18 vertical meters, with a mean of 823 grid cells per elevation band (maximum of 1412). *Rice et al.* [2011] found that snow disappearance in the Sierra Nevada occurred 20 days later for each 300 m rise in elevation. The 18 m elevation discretization captures this variability at approximately one day per elevation band. For each warmer scenario, the total annual meltwater volume is reported as the fraction of that simulated in the nominal (i.e., unperturbed) case. For all scenarios, we report the annual meltwater in three ways: the average meltwater volume and melt rate within each elevation band, the sum of annual meltwater within each elevation band, and the total annual meltwater summed over the entire model domain. The sensitivity of total domain-wide annual meltwater to simulated warming is examined with a (linear) regression analysis of the fraction of historical total meltwater for each warmer scenario of the three years.

To evaluate the effect of simulated warming on melt rates over the elevation profile for the three years, we report the elevation-specific mean fraction of total annual meltwater produced at high ($\geq$ 15 mm day^{-1}) melt rates, reported as a percent change relative to the nominal case. The 15 mm day^{-1} threshold was selected as a compromise between the 12.5 mm day^{-1} threshold

The Cryosphere Discuss., https://doi.org/10.5194/tc-2017-123
Manuscript under review for journal The Cryosphere
Discussion started: 18 July 2017

293 above which positive streamflow anomalies were reported by *Barnhart et al.* [2016] and a 20
294 mm day^{-1} classification of very heavy rainfall [*Klein Tank et al.*, 2009] used by *Musselman et al.*
295 [2017]. To examine how daily snowmelt rates respond to simulated warming, we present a
296 quantile analysis of the 25th, 50th, 75th, 90th, 95th, and 99th percentiles of daily snowmelt rates ≥ 1
297 mm day^{-1} from the warmer scenarios compared to those from the nominal case. Lastly, we
298 present an analysis of the meteorological conditions that control the response of snowmelt rates
299 to successive degrees of simulated warming.

300 **3. Results**

301 Maps of simulated SWE on 1 April, 1 May, and 1 June (Fig. 2) highlight seasonal and inter-
302 annual SWE patterns and illustrate the great variability of SWE with elevation. The lowest
303 elevations were consistently snow-free during the spring. Middle elevations included a transition
304 zone from snow-free to seasonally persistent snow-cover; that transition occurred at
305 progressively higher elevations later in the melt season and occurred earlier (later) in the drier
306 (wetter) snow years. The upper elevations contained the greatest SWE and most persistent spring
307 snow-cover (Fig. 2). The three-year observation period captured years with below-average
308 snowfall (2009; 23% below average SWE; hereafter 'moderately dry year'), average snowfall
309 (2008; 7% above average SWE; hereafter 'average year'), and above-average snowfall (2010;
310 54% above average SWE; hereafter 'moderately wet year') as determined from regional
311 automated SWE records (Fig. 3 and Table S1). The average (hourly) air temperature and
312 shortwave radiation values measured at the alpine Topaz Lake station in January-February-
313 March (JFM; the accumulation season) and April-May-June (AMJ; the melt season) provides
314 more insight into the meteorological differences amongst the three years. The drier and average

315 years exhibited similar average air temperatures, but the AMJ mean shortwave radiation was
316 lower in the moderately dry year (Table 2) due to higher spring cloud-cover (see Fig. 6 in
317 *Musselman et al.* [2012a]). The AMJ period in the moderately wet year was > 2°C colder than
318 the other years (Table 2) due to a series of large snowfall events in mid-April (Fig. 3) that
319 prolonged snow-cover (Fig. 2).

320 **3.1. Model evaluation against observation**

321 Compared to automated snow pillow SWE measurements, the model performed
322 favorably (RMSE ≤ 100 mm; bias better than ±85 mm) at all elevations in 2008 and 2010 (Fig.
323 3). In 2009, the model underestimated SWE compared to measurements made at the two higher
324 elevation stations, but accurately simulated SWE at the lower Giant Forest station (RMSE = 34
325 mm; bias = -4 mm) (Fig. 3). The greatest model error occurred at the Big Meadows station (2317
326 m asl) resulting from a significant underestimation of all snow events and errors were less at the
327 higher and lower elevation stations (Fig. 3). Despite this underestimation, in general, the SWE
328 magnitude and date of snow disappearance was well approximated by the model compared to the
329 automated station measurements.

330 Compared to the range of snow depth measured by six sensors at each of four sites in the
331 forested Wolverton basin, the model accurately captured the seasonal snow depth dynamics,
332 including maximum accumulation, the rate of depletion, and the date of snow disappearance
333 (Fig. 4; note that simulated snow depth is generally within the measurement envelope). The
334 general underestimation of SWE in 2009 was not apparent in the verification against the six
335 automated depth measurements at four sites in the Wolverton basin (Fig. 4).

336 The early-April surveys of the alpine Tokopah basin show 2009, 2008, and 2010 being
337 the drier (849±401 mm SWE), average (1000±476 mm SWE), and wetter (1265±310 mm SWE)
338 snow seasons, respectively (Table S2). Model SWE errors (NMSE) were highest during the melt
339 season when the measured variability was highest relative to the mean, and lowest during the
340 accumulation season (Table S2). On average, the forested Wolverton and alpine Tokopah basins
341 exhibited similar NMSE values of ~ 0.14 at maximum accumulation. In general, the model
342 tended to overestimate SWE with the exception of the February 2009 Wolverton survey, for
343 which modeled SWE was negatively biased (Table S2). The survey mean bias values were
344 typically much less than the standard deviation of the biases.
345 In general, model SWE errors were lower when evaluated against the CCSS snow course
346 measurements (Table S3) than the basin-wide survey measurements (Table S2). The large
347 underestimation of SWE in 2009 seen in the comparison against the automated SWE stations
348 (Fig. 3) is also seen in comparison to SWE measured at the two lowest elevation snow course
349 sites (Table S3). Conversely, comparison to the two highest elevation snow course sites indicated
350 a slight positive model bias in 2009. Overall, the model performed best in regions closest to
351 precipitation gauges used to force the model; SWE RMSE values were better explained by this
352 metric than by elevation alone (Fig. S1).

353 **3.2. Elevation-dependent SWE and snowmelt patterns**

354 The upper panels of Fig. 5 show the nominal simulations of the daily SWE and melt averaged
355 along elevation bands for the three years. Persistent seasonal snowpack was simulated >1800 m
356 asl in all years. Maximum annual SWE increased with elevation (colors in the top row panels of
357 Fig. 5); however, the date of maximum SWE exhibited a complex relationship with elevation,

The Cryosphere Discuss., https://doi.org/10.5194/tc-2017-123
Manuscript under review for journal The Cryosphere
Discussion started: 18 July 2017

358 snowfall magnitude and timing, and snowpack persistence that all varied amongst years (Fig. 5).
359 Generally, maximum SWE occurred later with increasing elevation but progressed in a step-wise
360 manner, often with little change over hundreds of vertical meters interspersed with abrupt jumps
361 of one to two months (Fig. 5).

362 Simulated daily melt was episodic in nature with the highest rates (> 35 mm day^{-1}; reds in
363 the bottom panels of Fig. 5) generally confined to elevations > 2000 m asl and the late-spring and
364 early summer. The highest elevations and years with more/later snow had the highest melt rates.
365 In all three years, winter melt was generally low (<5 mm day^{-1}) with rare, episodic, and more
366 intense melt events confined to lower elevations (Fig. 5).

367 **3.3. Elevation-dependent snowpack and snowmelt response to warming**

368 In the nominal case, the total meltwater volume summed over each elevation band was
369 consistently greatest between 2500 m and 2800 m asl (see Fig. 6; right panels), corresponding to
370 the peak in the regional hypsometry (see histograms in Fig. 1). Under the warmer scenarios, the
371 maximum meltwater volume, inferred from the peaks in Fig. 6, shifts upward in elevation by ~
372 600 m to the regional treeline (see Fig. 1). This upward elevation shift occurred under +2°C,
373 +3°C, and +4°C warming for the dry, average and wet snow seasons, respectively. Additional
374 warming reduced the total melt volume, but did not change the elevation at which the maximum
375 volume occurred.

376 Lower and middle elevations were prone to large reductions in the fraction of historical
377 meltwater volume (see line graphs in Fig. 6). At 2000 m asl, only 50% of the historical water in
378 the form of snow remained in a +3°C scenario, further reducing to 20% in the +5°C scenario.
379 Overall, snow at the upper elevations in the moderately dry snow season was more susceptible to

large reductions (Fig. 6). Conversely, upper elevation snowpack during the average and higher snowfall seasons was more resilient to warming. For example, at 2700 m asl, +1°C warming reduced annual meltwater volume by 1%, 3%, and 11% in the wetter, average and drier snow seasons, respectively; those values increased to 7%, 21% and 28% in the +3°C scenario.

Despite elevation-dependent nonlinear meltwater response to warming, the domain-total meltwater volume exhibited linear response to successive warming. Figure 7 shows linear regressions fit to the fraction of the nominal-case total meltwater for each scenario and year (see Table S4). The dry and average years were slightly more susceptible to warming (-10.5% to -10.8% change per °C) than the wetter year (-9.3% change per °C). Sublimation estimates ranged from 5% to 9% in the nominal case to 8% to 14% in the +6°C scenario (Table S4).

Warmer temperatures impact not only the total annual meltwater, but also the rate at which meltwater is produced. Figure 8 shows the fraction of the total meltwater per unit area over the elevation profile that is produced at high ($\geq$ 15 mm day^{-1}) melt rates; the complement of that fraction occurs at lower (<15 mm day^{-1}) rates. Consistently, meltwater production at upper elevations is dominated by high melt rates, while at lower elevations melt rates are predominately low. At ~ 2200 m asl, melt in the nominal cases occurred equally at low and high rates; above this middle elevation zone, melt occurs at high rates ($\geq$ 15 mm day^{-1}) and at low rates (<15 mm day^{-1}) below this elevation (see black circle markers in Fig. 8). Warming greatly decreases the fraction of meltwater produced at high melt rates and increases that produced at low rates (see lower colored graphs in Fig. 8). As a result, the elevation at which meltwater is produced equally at low and high rates is pushed upward by ~150 m °C^{-1} (Fig. 8). The greatest melt rate reductions occur at forested elevations with generally lesser change in alpine areas above ~ 3300 m asl.

The Cryosphere Discuss., https://doi.org/10.5194/tc-2017-123
Manuscript under review for journal The Cryosphere
Discussion started: 18 July 2017

There is a general tendency toward lower snowmelt rates in response to successive warming with the lower elevations and the year with the most snowfall (and latest storm events) prone to the greatest reductions (Fig. 9). There are notable exceptions. Extreme melt rates (99^{th} percentiles; downward-facing triangles in Fig. 9) actually increase (inferred from markers plotting above the 1:1 line) at elevations > 2800 m asl in all years (top panels) and in the drier year at all elevations (left panels). To better understand why these extreme melt rates differ in trend from the lower percentiles, we provide a brief analysis of 2009 extreme melt events. The analysis is limited to elevations above 2250 m asl where a threshold of 40 mm day^{-1} designates extreme (99^{th} percentiles) melt rates (see Fig. 9).

In the spring, extreme melt affected a very limited portion of the domain on any given day (inferred from blue colors on the right in the top panel of Fig. 10), and the spatial extent of extreme melt generally decreased in response to warming. Conversely, three distinct extreme melt events on 21 January, 22 February, and 1 March 2009 (arrows in Fig. 10) exhibit large increases in the fraction of the domain affected, with the January and March events increasing in spatial extent until +4°C before decreasing with additional warming. The simulated melt events were not associated with substantial rainfall, but rather cloudy and/or windy conditions with high longwave radiation that generally occurred under warmer-than-average temperatures in the nominal case. Measured meteorological conditions for these days are provided in Table 3. These warm and cloudy winter conditions were insufficient to produce widespread extreme melt in the nominal case; melt was limited to elevations < 2000 m asl and generally did not exceed the 99^{th} percentile (Table 3). Additional warming caused extreme rates of melt to occur at increasingly higher elevations at a time of substantial snow-cover (Fig. 10).

4. Discussion

426 Our results confirm that climate warming will have uneven effects on the California
427 landscape [*Cayan et al.*, 2008] and that elevation is a critical determinant of snowpack – climate
428 sensitivity. Despite the simplicity of our climate sensitivity method, the predicted sensitivity of
429 total snow volume to warming of -9.3% to -10.8% $°C^{-1}$ is consistent with previous studies using
430 either statistical and dynamical downscaling of GCM output (*Sun et al.* [2016]; -9.3% $°C^{-1}$) or a
431 simple statistical snow model trained on observations (*Howat and Tulaczyk* [2005]; -10% $°C^{-1}$).
432 The consistency suggests that these models of varying complexity adequately treat the warming-
433 induced shift from snowfall to rain. This confirms recent findings by *Schlögl et al.* [2016] that
434 snow model errors may be negligible when relative climate sensitivity metrics are evaluated.
435 Further, we show linearity in the sensitivity of domain-wide annual meltwater volume to
436 successive degrees of warming. The year with the most snowfall, characterized by late snowfall
437 events and cold spring (AMJ) air temperatures, was slightly more resilient (-9.3% $°C^{-1}$) to
438 warming than the drier or average snow years. In a study of the sensitivity of snow to warming in
439 Mediterranean climates, including the Tokopah basin, *López-Moreno et al.* [2017] report that
440 simulated changes in precipitation magnitude (±20%) did not affect the relative snowpack
441 climate sensitivity to warming. Thus, snowmelt rates may be more sensitive to changes in the
442 seasonal timing of precipitation than to changes in precipitation magnitude. This supports the
443 conclusions of *Cooper et al.* [2016] that record low snowpack years may not serve as appropriate
444 analogues for the climate sensitivity of snow.
445 In a warmer climate, shifts from snowfall to rain are likely to combine with shifts in
446 snowmelt timing to cause earlier water availability relative to the historical period. As a result,
447 the ephemeral snow zone is expected to progress upward in elevation [*Minder*, 2010] and shift
448 the areal distribution of SWE toward higher, unmonitored elevations. Indeed, the +3°C scenario

449 shifted the elevation of maximum annual meltwater volume above that of the highest regional
450 SWE observing station. The results confirm previous findings in the U.S. Pacific Northwest that
451 the current observing network design may be insufficient in a warmer world [*Gleason et al.*,
452 2017]. Warmer temperatures and earlier melt timing [*Stewart et al.*, 2004] also influence the rate
453 of meltwater production [*Musselman et al.*, 2017], a critical determinant of streamflow [*Barnhart*
454 *et al.*, 2016], forest carbon uptake [*Winchell et al.*, 2016], and flood hazard [*Hamlet and*
455 *Lettenmaier*, 2007]. Despite a strong negative relationship between temperature and elevation,
456 we show a positive relationship between elevation and seasonal snowmelt rates. Compared to
457 earlier melt at lower elevations, later snowmelt at upper elevations was more rapid due largely to
458 higher solar insolation coincident with later melt [*Musselman et al.*, 2012a]. Prolonged snow-
459 cover at upper, compared to lower elevations, and in wetter, compared to drier snow seasons, is
460 an important factor in interpreting snowmelt temperature sensitivity results.

461 We show a general tendency toward lower melt rates in response to warming. In contrast
462 to *Musselman et al.* [2017], which evaluated mean snowmelt response to a single greenhouse gas
463 emissions scenario at 4 km resolution, we evaluate a range of potential warming, examine the
464 percentile distribution of snowmelt response, and elucidate the process along elevational
465 gradients most relevant to basin-wide runoff. This is a critical advancement in understanding
466 how and where meltwater production is impacted by warming; an evaluation that cannot be
467 achieved with the type of 'high-resolution' climate modeling used in *Musselman et al.* [2017].
468 Importantly, we report an emergence (i.e., not present in the historical simulations) and spatial
469 expansion of extreme winter melt events and, conversely, a decline in extreme melt during
470 spring. Increases in extreme winter melt occurred under warm and cloudy conditions, and
471 decreases in extreme spring melt was due to reduced snow-cover persistence. This is an

472 important new finding with implications on flood hazard and reservoir management. The general
473 tendency toward slower snowmelt rates and higher extreme values is analogous to the expected
474 climate change impacts on precipitation, where high-intensity events are expected to increase
475 despite projected declines in total (e.g., summer) precipitation [*Prein et al.*, 2016; *Trenberth*,
476 2011].

477 Increases in extreme winter melt rates, combined with a greater proportion of
478 precipitation falling as rain could locally increase winter flood risk. Higher winter runoff
479 complicates reservoir management faced with competing objectives to maintain flood control
480 storage capacity during winter and to maximize water storage during spring in preparation for the
481 arid summer. In this context, substantial winter runoff may have to be released downstream
482 thereby reducing summer water storage required for agriculture, fish and wildlife management,
483 hydropower production, recreation, water quality and municipal supply [*Lettenmaier et al.*,
484 1999]. We show that historical extreme melt rates (99^{th} percentiles) impact a relatively limited
485 area (generally <30% of land area above 2250 m asl) at any given time. This is likely due to
486 snowpack cold content and/or cool air temperatures limiting melt at upper elevations and low
487 snow-cover fraction limiting melt at lower elevations. Compared to the historical period,
488 warming doubles the basin area undergoing extreme melt, and shifts its occurrence from spring
489 to winter. The increased spatial extent, intensity, and frequency of extreme winter snowmelt
490 events may have significant implications for antecedent moisture conditions and associated flood
491 risk.

492 Snowmelt rates have been mechanistically linked to streamflow production [*Barnhart et*
493 *al.*, 2016], but less-understood are the potential implications of climate-induced changes in
494 snowmelt rates on subsurface water storage, evapotranspiration and streamflow response. For

example, recent empirical evidence that a precipitation shift from snow towards rain will lead to a decrease in streamflow [*Berghuijs et al.*, 2014] lacks definitive causation. Compared to soil, snow-cover exhibits different water routing mechanisms. For example, lateral downslope flow of water along snowpack layers has been shown to explain the observed rapid delivery of water to streams and anomalously high contributions of event water to the hydrograph during rain-on-snow and snowmelt [*Eiriksson et al.*, 2013]. One hypothesis is that as snow-cover becomes less persistent in a warmer world, and snowmelt rates decline, this rapid slope-scale redistribution of water toward stream channels will slow or cease, increasing the soil residence time of water. Longer soil residence time can increase the partitioning of water to evapotranspiration, and thus decrease streamflow.

Other empirical and modeling studies have reported declines in summertime streamflow due to earlier snowmelt runoff and earlier depletion of shallow aquifers [*Huntington and Niswonger*, 2012; *Luce and Holden*, 2009]. Catchment wetness (i.e., soil moisture content and shallow groundwater levels) has substantial impact on runoff response in mountainous areas with distinct thresholds determining relationships amongst wetness, streamflow, and contributing area [*Penna et al.*, 2011]; behavior controlled by soil type, subsurface storage capacity, and climate. These factors are also important drivers of evapotranspiration [*Christensen et al.*, 2008; *Lundquist and Loheide*, 2011] and the regional variability of hydrologic sensitivity to climate change [*Tague et al.*, 2008]. In this regard, percentage reductions in future streamflow may be more substantial than the meltwater reductions reported here because slower snowmelt is less efficient at generating streamflow.

Improved model error characterization for the baseline (nominal) years is a critical step toward informed interpretation of the results of our climate change sensitivity analysis. While

518 snow model errors may be negligible when relative climate sensitivity metrics are evaluated
519 [*Schlögl et al.*, 2016], runoff simulations require accurate representation of snowpack volume
520 and melt rates. Simulated snow depth values were within the range of observations from
521 automated sensors at four sites spanning elevation, forest density, slope and aspect. This
522 verification provides confidence in the model to capture accumulation, melt rates, and the date of
523 snow disappearance across spatial and temporal scales. Notwithstanding, there are inherent
524 strengths and weaknesses of the different validation data sets. For example, the basin-scale
525 survey design samples only three snow depth measurement points within a given grid cell.
526 Similarly, the automated stations only sample a single point. The degree to which these point
527 samples represent the average value over an area consistent with the model grid scale is a source
528 of inherent discrepancy between models and observations, independent of model skill [*Trujillo*
529 *and Lehning*, 2015]. Overall, the model performed best in regions closest to precipitation gauges
530 used to force the model (Fig. S1) and tended to slightly overestimate SWE at upper elevations
531 (Table S3).

532 Our assumption of a uniform temperature perturbation does not consider changes in
533 climate dynamics at diurnal (e.g., nighttime vs. daytime temperature changes), synoptic (e.g.,
534 number of cool vs. warm days), or seasonal (e.g., winter vs. spring temperature changes) scales.
535 These interactions may be best characterized using GCM output dynamically downscaled to fine-
536 resolutions with regional climate models [e.g., *Liu et al.*, 2016; *Sun et al.*, 2016] or within a
537 delta-change approach that considers the range of uncertainties in the climate change signal of
538 different emissions scenarios [e.g., *Marty et al.*, 2017]. By not addressing the snow-albedo
539 feedback between snow-cover depletion and warmer temperatures [*Letcher and Minder*, 2015;
540 *Pepin and Lundquist*, 2008], it is possible that we underestimate regional air temperature

changes toward the end of the melt season in the warmer scenarios. Such negative temperature biases would cause underestimation of the snow depletion rate and, ultimately, the snowpack sensitivity to warming. However, these biases may be partially mitigated by our assumption that the winter and spring, and nighttime and daytime, air temperatures warm uniformly.

Sublimation estimates of 5% to 9% in the nominal case to 8% to 14% in the +6°C scenario (Table S4) are on the lower- to middle-end of the reported regional values of 2% to 3% [*West and Knoerr*, 1959] to 20% [*Marks and Dozier*, 1992]. The large range highlights challenges and disparities in measuring [e.g., *Molotch et al.*, 2007; *Sexstone et al.*, 2016] and modeling [*Etchevers et al.*, 2004] turbulent exchange, which are further compounded in mountainous terrain due to the challenges of windflow simulation [*Musselman et al.*, 2015]. By not considering blowing snow and subsequent sublimation losses (i.e., overestimating alpine snowpack), we may further underestimate snowpack sensitivity to warming.

In light of the potential errors discussed above, our results should be considered somewhat conservative. Longer-term snow and runoff simulations at scales sufficient to resolve mountain climate elevation gradients are needed both as reanalysis to understand historical conditions [e.g., snow reanalysis by *Margulis et al.*, 2016], and forced by large suites of future climate scenarios [e.g., *Eyring et al.*, 2016] that dynamically resolve different model realizations of climate response to different greenhouse gas emissions scenarios. Such efforts will best inform, and constrain the uncertainty of, potential impacts of climate change on flood risk and water availability. Toward this goal, our work makes inroads to quantify how snowpack and melt dynamics respond to incremental warming over an elevation profile characteristic of a foothills-to-headwaters mountain front. The results offer insight into the sensitivity of snow water

563 resources to climate change in the Sierra Nevada, California, with implications for other regions
564 as well.

565 5. Conclusions

566 We present a climate sensitivity experiment to investigate how historical snow water resources
567 and melt rates respond to successively warmer temperatures over a large elevation gradient in the
568 southern Sierra Nevada, California. Good agreement between simulations and an unprecedented
569 array of ground-based observations of SWE (RMSE ≤ 100 mm; bias better than ±85 mm) and
570 snow depth (within multi-sensor range) is shown. Three primary findings emerge from the
571 simulations. First, the sensitivity of total snow-water volume to warming is -9.3% to -10.8% per
572 °C. The snow season characterized by above-average snowfall and cold spring storm events was
573 most resilient to warming; however, it also exhibited the greatest shift toward slower melt. Thus,
574 snowmelt rates may be more sensitive to changes in the seasonal timing of precipitation than to
575 changes in precipitation magnitude. Second, the middle elevations, which are dominated by
576 forest cover and comprise a disproportionately large basin area, exhibit the greatest snowpack
577 reductions and the largest shift toward slower snowmelt. Hence, warming-related impacts on
578 runoff production and ecosystem function may be particularly acute in these areas. Third,
579 increases in the frequency, intensity, and spatial extent of extreme winter melt events occur with
580 successive warming. Warming-induced extreme (winter) melt impacts an area nearly twice as
581 large as that simulated at any time in the historical period. The changes in extreme snowmelt
582 events have implications for antecedent moisture conditions and associated flood risk. When
583 considered together, the elevation-dependent climate sensitivity of snowmelt revealed herein has
584 broad implications for water supply monitoring, streamflow production, flood control, and
585 ecosystem function in a warmer world.

Acknowledgements

The authors thank Sequoia National Park for support of research efforts. Financial support was provided by the National Science Foundation grants EAR-1032295, EAR-1032308, and EAR-1246473, the Southern Sierra Critical Zone Observatory (EAR-0725097), a Major Research Instrumentation grant (EAR-0619947), and the Mountain Research Initiative. The first author was supported by a National Aeronautics and Space Administration (NASA) Earth System Science Fellowship. R. Bales and P. Kirchner supported hydrometeorological infrastructure in the Wolverton basin. J. Sickman and J. Melack provided solar radiation and snow survey data from the Tokopah basin. Alpine3D is provided the WSL Swiss Federal Institute for Snow and Avalanche Research SLF (online: https://models.slf.ch/p/alpine3d/downloads/). Special thanks goes to M. Lehning and M. Bavay. Model forcing data are freely available online from the agencies listed in Table 1. Land-cover and validation data are either available online from sources referenced in the text, or are otherwise provided in the figures, tables, and supplements. The authors are grateful to everyone who provided field assistance including: K. Skeen, S. Roberts, B. Forman, D. Perrot, E. Trujillo, L. Meromy, M. Girotto, A. Kahl, K. Ritger, N. Bair, D. Berisford, A. Kinoshita, and M. Cooper.

References

Bales, R. C., N. P. Molotch, T. H. Painter, M. D. Dettinger, R. Rice, and J. Dozier (2006), Mountain hydrology of the western United States, *Water Resour. Res.*, *42*(8), W08432.

Barnett, T. P., J. C. Adam, and D. P. Lettenmaier (2005), Potential impacts of a warming climate on water availability in snow-dominated regions, *Nature*, *438*(7066), 303-309.

Barnhart, T. B., N. P. Molotch, B. Livneh, A. A. Harpold, J. F. Knowles, and D. Schneider (2016), Snowmelt rate dictates streamflow, *Geophysical Research Letters*, *43*(15), 8006-8016.

Bartelt, P., and M. Lehning (2002), A physical SNOWPACK model for the Swiss avalanche warning: Part I: numerical model, *Cold Regions Science and Technology*, *35*(3), 123-145.

Bavay, M., and T. Egger (2014), MeteoIO 2.4. 2: a preprocessing library for meteorological data, *Geoscientific Model Development*, *7*(6), 3135-3151.

Bavay, M., T. Grünewald, and M. Lehning (2013), Response of snow cover and runoff to climate change in high Alpine catchments of Eastern Switzerland, *Advances in Water Resources*, *55*, 4-16.

Bavay, M., M. Lehning, T. Jonas, and H. Löwe (2009), Simulations of future snow cover and discharge in Alpine headwater catchments, *Hydrological Processes*, *23*(1), 95-108.

Berghuijs, W., R. Woods, and M. Hrachowitz (2014), A precipitation shift from snow towards rain leads to a decrease in streamflow, *Nat. Clim. Change*, *4*(7), 583-586.

Brown, R. D., and P. W. Mote (2009), The response of northern hemisphere snow cover to a changing climate*, *Journal of Climate*, *22*(8), 2124-2145.

Cayan, D. R., E. P. Maurer, M. D. Dettinger, M. Tyree, and K. Hayhoe (2008), Climate change scenarios for the California region, *Climatic change*, *87*, 21-42.

Christensen, L., C. L. Tague, and J. S. Baron (2008), Spatial patterns of simulated transpiration response to climate variability in a snow dominated mountain ecosystem, *Hydrological Processes*, *22*(18), 3576-3588.

Cooper, M. G., A. W. Nolin, and M. Safeeq (2016), Testing the recent snow drought as an analog for climate warming sensitivity of Cascades snowpacks, *Environmental Research Letters*, *11*(8), 084009.

Dettinger, M. (2011), Climate Change, Atmospheric Rivers, and Floods in California–A Multimodel Analysis of Storm Frequency and Magnitude Changes, *JAWRA Journal of the American Water Resources Association*, *47*(3), 514-523.

Dettinger, M. D., and D. R. Cayan (1995), Large-scale atmospheric forcing of recent trends toward early snowmelt runoff in California, *Journal of Climate*, *8*(3), 606-623.

Dettinger, M. D., D. R. Cayan, M. K. Meyer, and A. E. Jeton (2004), Simulated hydrologic responses to climate variations and change in the Merced, Carson, and American River basins, Sierra Nevada, California, 1900–2099, *Climatic Change*, *62*(1-3), 283-317.

Eiriksson, D., M. Whitson, C. H. Luce, H. P. Marshall, J. Bradford, S. G. Benner, T. Black, H. Hetrick, and J. P. McNamara (2013), An evaluation of the hydrologic relevance of lateral flow in snow at hillslope and catchment scales, *Hydrological Processes*, *27*(5), 640-654.

Elder, K., J. Dozier, and J. Michaelsen (1988), Spatial and temporal variation of net snow accumulation in a small alpine watershed, Emerald Lake basin, Sierra Nevada, California, USA, *Annals of Glaciology*, *13*, 56-63.

Etchevers, P., E. Martin, R. Brown, C. Fierz, Y. Lejeune, E. Bazile, A. Boone, Y.-J. Dai, R. Essery, and A. Fernandez (2004), Validation of the energy budget of an alpine snowpack simulated by several snow models (SnowMIP project), *Annals of Glaciology*, *38*(1), 150-158.

Eyring, V., S. Bony, G. A. Meehl, C. A. Senior, B. Stevens, R. J. Stouffer, and K. E. Taylor (2016), Overview of the Coupled Model Intercomparison Project Phase 6 (CMIP6) experimental design and organization, *Geoscientific Model Development*, *9*(5), 1937-1958.

Fry, J. A., G. Xian, S. Jin, J. A. Dewitz, C. G. Homer, Y. LIMIN, C. A. Barnes, N. D. Herold, and J. D. Wickham (2011), Completion of the 2006 national land cover database for the conterminous United States, *Photogrammetric Engineering and Remote Sensing*, *77*(9), 858-864.

Fyfe, J. C., C. Derksen, L. Mudryk, G. M. Flato, B. D. Santer, N. C. Swart, N. P. Molotch, X. Zhang, H. Wan, and V. K. Arora (2017), Large near-term projected snowpack loss over the western United States, *Nature Communications*, *8*.

Girotto, M., S. A. Margulis, and M. Durand (2014a), Probabilistic SWE reanalysis as a generalization of deterministic SWE reconstruction techniques, *Hydrological Processes*, *28*(12), 3875-3895.

Girotto, M., G. Cortés, S. A. Margulis, and M. Durand (2014b), Examining spatial and temporal variability in snow water equivalent using a 27 year reanalysis: Kern River watershed, Sierra Nevada, *Water Resources Research*, *50*(8), 6713-6734.

Gleason, K. E., A. W. Nolin, and T. R. Roth (2017), Developing a representative snow-monitoring network in a forested mountain watershed, *Hydrology and Earth System Sciences*, *21*(2), 1137.

Gleick, P. H. (1987), The development and testing of a water balance model for climate impact assessment: modeling the Sacramento basin, *Water Resources Research*, *23*(6), 1049-1061.

Gleick, P. H., and E. L. Chalecki (1999), THE IMPACTS OF CLIMATIC CHANGES FOR WATER RESOURCES OF THE COLORADO AND SACRAMENTO‐SAN JOAQUIN RIVER BASINS1, *JAWRA Journal of the American Water Resources Association*, *35*(6), 1429-1441.

Godsey, S., J. Kirchner, and C. Tague (2013), Effects of changes in winter snowpacks on summer low flows: case studies in the Sierra Nevada, California, USA, *Hydrological Processes*.

Hamlet, A. F., and D. P. Lettenmaier (2007), Effects of 20th century warming and climate variability on flood risk in the western US, *Water Resources Research*, *43*(6).

Howat, I. M., and S. Tulaczyk (2005), Climate sensitivity of spring snowpack in the Sierra Nevada, *Journal of Geophysical Research: Earth Surface*, *110*(F4).

Hunsaker, C. T., T. W. Whitaker, and R. C. Bales (2012), Snowmelt runoff and water yield along elevation and temperature gradients in California's Southern Sierra Nevada1, edited, Wiley Online Library.

Huntington, J. L., and R. G. Niswonger (2012), Role of surface‐water and groundwater interactions on projected summertime streamflow in snow dominated regions: An integrated modeling approach, *Water Resources Research*, *48*(11).

Jepsen, S. M., N. P. Molotch, M. W. Williams, K. E. Rittger, and J. O. Sickman (2012), Interannual variability of snowmelt in the Sierra Nevada and Rocky Mountains, United States: Examples from two alpine watersheds, *Water Resources Research*, *48*(2).

689 Klein Tank, A., F. W. Zwiers, and X. Zhang (2009), Guidelines on analysis of extremes in a
690 changing climate in support of informed decisions for adaptation, edited by C. D. a.
691 Monitoring, p. 56, World Meteorological Organization.
692 Knowles, N., and D. R. Cayan (2002), Potential effects of global warming on the
693 Sacramento/San Joaquin watershed and the San Francisco estuary, *Geophysical Research*
694 *Letters*, *29*(18), 38-31-38-34.
695 Knowles, N., and D. R. Cayan (2004), Elevational dependence of projected hydrologic changes
696 in the San Francisco estuary and watershed, *Climatic Change*, *62*(1-3), 319-336.
697 Knowles, N., M. D. Dettinger, and D. R. Cayan (2006), Trends in Snowfall versus Rainfall in the
698 Western United States, *Journal of Climate*, *19*(18), 4545-4559.
699 Kobierska, F., T. Jonas, M. Zappa, M. Bavay, J. Magnusson, and S. M. Bernasconi (2013),
700 Future runoff from a partly glacierized watershed in Central Switzerland: a two-model
701 approach, *Advances in Water Resources*, *55*, 204-214.
702 Kobierska, F., T. Jonas, J. Magnusson, M. Zappa, M. Bavay, T. Bosshard, F. Paul, and S. M.
703 Bernasconi (2011), Climate change effects on snow melt and discharge of a partly glacierized
704 watershed in Central Switzerland (SoilTrec Critical Zone Observatory), *Applied*
705 *Geochemistry*, *26, Supplement*(0), S60-S62.
706 Lehning, M., I. Völksch, D. Gustafsson, T. A. Nguyen, M. Stähli, and M. Zappa (2006),
707 ALPINE3D: a detailed model of mountain surface processes and its application to snow
708 hydrology, *Hydrological Processes*, *20*(10), 2111-2128.
709 Letcher, T. W., and J. R. Minder (2015), Characterization of the Simulated Regional Snow
710 Albedo Feedback Using a Regional Climate Model over Complex Terrain, *Journal of*
711 *Climate*, *28*(19), 7576-7595.
712 Lettenmaier, D. P., and T. Y. Gan (1990), Hydrologic sensitivities of the Sacramento‐San
713 Joaquin River Basin, California, to global warming, *Water Resources Research*, *26*(1), 69-
714 86.
715 Lettenmaier, D. P., A. W. Wood, R. N. Palmer, E. F. Wood, and E. Z. Stakhiv (1999), Water
716 resources implications of global warming: A US regional perspective, *Climatic Change*,
717 *43*(3), 537-579.
718 Liston, G. E., and K. Elder (2006), A Meteorological Distribution System for High-Resolution
719 Terrestrial Modeling (MicroMet), *Journal of Hydrometeorology*, *7*(2), 217-234.
720 Liu, C., K. Ikeda, R. Rasmussen, M. Barlage, A. J. Newman, A. F. Prein, F. Chen, L. Chen, M.
721 Clark, and A. Dai (2016), Continental-scale convection-permitting modeling of the current
722 and future climate of North America, *Climate Dynamics*, 1-25.
723 López-Moreno, J. I., S. Fassnacht, J. Heath, K. Musselman, J. Revuelto, J. Latron, E. Morán-
724 Tejeda, and T. Jonas (2013), Small scale spatial variability of snow density and depth over
725 complex alpine terrain: Implications for estimating snow water equivalent, *Advances in*
726 *Water Resources*, *55*, 40-52.
727 López-Moreno, J. I., et al. (2017), Different sensitivities of snowpacks to warming in
728 Mediterranean climate mountain areas, *Environmental Research Letters*.
729 Luce, C. H., and Z. A. Holden (2009), Declining annual streamflow distributions in the Pacific
730 Northwest United States, 1948–2006, *Geophysical Research Letters*, *36*(16).
731 Lundquist, J. D., and S. P. Loheide (2011), How evaporative water losses vary between wet and
732 dry water years as a function of elevation in the Sierra Nevada, California, and critical factors
733 for modeling, *Water Resources Research*, *47*(3).

734 Magnusson, J., D. Farinotti, T. Jonas, and M. Bavay (2011), Quantitative evaluation of different
735 hydrological modelling approaches in a partly glacierized Swiss watershed, *Hydrological*
736 *Processes*, *25*(13), 2071-2084.
737 Margulis, S. A., G. Cortés, M. Girotto, and M. Durand (2016), A Landsat-Era Sierra Nevada
738 Snow Reanalysis (1985–2015), *Journal of Hydrometeorology*, *17*(4), 1203-1221.
739 Marks, D., and J. Dozier (1992), Climate and energy exchange at the snow surface in the alpine
740 region of the Sierra Nevada: 2. Snow cover energy balance, *Water Resources Research*,
741 *28*(11), 3043-3054.
742 Marks, D., J. Dozier, and R. E. Davis (1992), Climate and energy exchange at the snow surface
743 in the Alpine Region of the Sierra Nevada: 1. Meteorological measurements and monitoring,
744 *Water Resour. Res.*, *28*(11), 3029-3042.
745 Marty, C., S. Schlögl, M. Bavay, and M. Lehning (2017), How much can we save? Impact of
746 different emission scenarios on future snow cover in the Alps, *The Cryosphere*, *11*(1), 517.
747 McCabe, G. J., and M. P. Clark (2005), Trends and variability in snowmelt runoff in the western
748 United States, *Journal of Hydrometeorology*, *6*(4), 476-482.
749 Michlmayr, G., M. Lehning, G. Koboltschnig, H. Holzmann, M. Zappa, R. Mott, and W.
750 Schöner (2008), Application of the Alpine 3D model for glacier mass balance and glacier
751 runoff studies at Goldbergkees, Austria, *Hydrological Processes*, *22*(19), 3941-3949.
752 Minder, J. R. (2010), The Sensitivity of Mountain Snowpack Accumulation to Climate
753 Warming, *Journal of Climate*, *23*(10), 2634-2650.
754 Molotch, N., M. Colee, R. Bales, and J. Dozier (2005), Estimating the spatial distribution of
755 snow water equivalent in an alpine basin using binary regression tree models: the impact of
756 digital elevation data and independent variable selection, *Hydrological Processes*, *19*(7),
757 1459-1479.
758 Molotch, N. P., and L. Meromy (2014), Physiographic and climatic controls on snow cover
759 persistence in the Sierra Nevada Mountains, *Hydrological Processes*, *28*(16), 4573-4586.
760 Molotch, N. P., P. D. Blanken, M. W. Williams, A. A. Turnipseed, R. K. Monson, and S. A.
761 Margulis (2007), Estimating sublimation of intercepted and sub-canopy snow using eddy
762 covariance systems, *Hydrological Processes*, *21*(12), 1567-1575.
763 Mote, P. W., A. F. Hamlet, M. P. Clark, and D. Lettenmaier (2005), Declining mountain
764 snowpack in western North America, *B Am Meteorol Soc*, *86*, 39-49.
765 Mott, R., F. Faure, oise, M. Lehning, H. we, B. Hynek, G. Michlmayer, A. Prokop, Sch, and W.
766 ner (2008), Simulation of seasonal snow-cover distribution for glacierized sites on Sonnblick,
767 Austria, with the Alpine3D model, *Annals of Glaciology*, *49*(1), 155-160.
768 Musselman, K. N., J. W. Pomeroy, R. L. Essery, and N. Leroux (2015), Impact of windflow
769 calculations on simulations of alpine snow accumulation, redistribution and ablation,
770 *Hydrological Processes*, *29*(18), 3983-3999.
771 Musselman, K. N., N. P. Molotch, S. A. Margulis, P. Kirchner, and R. C. Bales (2012a),
772 Influence of canopy structure and direct beam solar irradiance on snowmelt rates in a mixed
773 conifer forest, *Agricultural and Forest Meteorology*, *161C*, 46-56.
774 Musselman, K. N., N. P. Molotch, S. A. Margulis, M. Lehning, and D. Gustafsson (2012b),
775 Improved snowmelt simulations with a canopy model forced with photo-derived direct beam
776 canopy transmissivity, *Water Resour. Res.*, *48*(10).
777 Musselman, K. N., M. P. Clark, C. Liu, K. Ikeda, and R. Rasmussen (2017), Slower snowmelt in
778 a warmer world, *Nature Clim. Change*, *7*(3), 214-219.

779 Nolin, A. W., and C. Daly (2006), Mapping "at risk" snow in the Pacific Northwest, *J*
780 *Hydrometeorol*, *7*(5), 1164-1171.
781 NPS (2017), Sequoia and Kings Canyon National Park, Weather and Climate, Online:
782 https://www.nps.gov/seki/learn/education/climate.htm. Accessed 6/9/2017.
783 Penna, D., H. J. Tromp-van Meerveld, A. Gobbi, M. Borga, and G. Dalla Fontana (2011), The
784 influence of soil moisture on threshold runoff generation processes in an alpine headwater
785 catchment, *Hydrol. Earth Syst. Sci.*, *15*(3), 689-702.
786 Pepin, N., and J. Lundquist (2008), Temperature trends at high elevations: patterns across the
787 globe, *Geophysical Research Letters*, *35*(14).
788 Perrot, D., N. P. Molotch, M. W. Williams, S. M. Jepsen, and J. O. Sickman (2014),
789 Relationships between stream nitrate concentration and spatially distributed snowmelt in
790 high‐elevation catchments of the western US, *Water Resources Research*, *50*(11), 8694-
791 8713.
792 Prein, A. F., R. M. Rasmussen, K. Ikeda, C. Liu, M. P. Clark, and G. J. Holland (2016), The
793 future intensification of hourly precipitation extremes, *Nature Climate Change*.
794 Rasouli, K., J. W. Pomeroy, and D. G. Marks (2015), Snowpack sensitivity to perturbed climate
795 in a cool mid‐latitude mountain catchment, *Hydrological Processes*, *29*(18), 3925-3940.
796 Rice, R., R. C. Bales, T. H. Painter, and J. Dozier (2011), Snow water equivalent along elevation
797 gradients in the Merced and Tuolumne River basins of the Sierra Nevada, *Water Resources*
798 *Research*, *47*(8).
799 Rutter, N., et al. (2009), Evaluation of forest snow processes models (SnowMIP2), *J Geophys*
800 *Res-Atmos*, *114*, -.
801 Schlögl, S., C. Marty, M. Bavay, and M. Lehning (2016), Sensitivity of Alpine3D modeled snow
802 cover to modifications in DEM resolution, station coverage and meteorological input
803 quantities, *Environmental Modelling & Software*, *83*, 387-396.
804 Seager, R., M. Ting, C. Li, N. Naik, B. Cook, J. Nakamura, and H. Liu (2013), Projections of
805 declining surface-water availability for the southwestern United States, *Nature Climate*
806 *Change*, *3*(5), 482-486.
807 Sexstone, G. A., D. W. Clow, D. I. Stannard, and S. R. Fassnacht (2016), Comparison of
808 methods for quantifying surface sublimation over seasonally snow‐covered terrain,
809 *Hydrological Processes*, *30*(19), 3373-3389.
810 Sickman, J. O., A. Leydecker, C. C. Chang, C. Kendall, J. M. Melack, D. M. Lucero, and J.
811 Schimel (2003), Mechanisms underlying export of N from high-elevation catchments during
812 seasonal transitions, *Biogeochemistry*, *64*(1), 1-24.
813 Stewart, I. T., D. R. Cayan, and M. D. Dettinger (2004), Changes in snowmelt runoff timing in
814 western North America under abusiness as usual climate change scenario, *Climatic Change*,
815 *62*(1-3), 217-232.
816 Stocker, T. F., D. Qin, G.-K. Plattner, M. Tignor, S. K. Allen, J. Boschung, A. Nauels, Y. Xia, V.
817 Bex, and P. M. Midgley (2013), Climate Change 2013. The Physical Science Basis. Working
818 Group I Contribution to the Fifth Assessment Report of the Intergovernmental Panel on
819 Climate Change-Abstract for decision-makers, Groupe d'experts intergouvernemental sur
820 l'evolution du climat/Intergovernmental Panel on Climate Change-IPCC, C/O World
821 Meteorological Organization, 7bis Avenue de la Paix, CP 2300 CH-1211 Geneva 2
822 (Switzerland).
823 Sturm, M., M. A. Goldstein, and C. Parr (2017), Water and life from snow: A trillion dollar
824 science question, *Water Resources Research*.

Sun, F., A. Hall, M. Schwartz, D. B.Walton, and N. Berg (2016), Twenty-First-Century Snowfall and Snowpack Changes over the Southern California Mountains, *Journal of Climate*, *29*(1), 91-110.

Tague, C., and H. Peng (2013), The sensitivity of forest water use to the timing of precipitation and snowmelt recharge in the California Sierra: Implications for a warming climate, *Journal of Geophysical Research: Biogeosciences*, *118*(2), 875-887.

Tague, C., G. Grant, M. Farrell, J. Choate, and A. Jefferson (2008), Deep groundwater mediates streamflow response to climate warming in the Oregon Cascades, *Climatic Change*, *86*(1-2), 189-210.

Tonnessen, K. A. (1991), The Emerald Lake watershed study: introduction and site description, *Water Resour. Res.*, *27*(7), 1537-1539.

Trenberth, K. E. (2011), Changes in precipitation with climate change, *Climate Research*, *47*(1-2), 123-138.

Trujillo, E., and N. P. Molotch (2014), Snowpack regimes of the Western United States, *Water Resources Research*, *50*(7), 5611-5623.

Trujillo, E., and M. Lehning (2015), Theoretical analysis of errors when estimating snow distribution through point measurements, *The Cryosphere*, *9*(3), 1249-1264.

Trujillo, E., N. P. Molotch, M. L. Goulden, A. E. Kelly, and R. C. Bales (2012), Elevation-dependent influence of snow accumulation on forest greening, *Nature Geoscience*, *5*(10), 705-709.

Van Oldenborgh, G., M. Collins, J. Arblaster, J. Christensen, J. Marotzke, S. Power, M. Rummukainen, T. Zhou, T. Stocker, and D. Qin (2013), Annex I: Atlas of global and regional climate projections, *Climate change*, 1311-1393.

Vano, J. A., B. Udall, D. R. Cayan, J. T. Overpeck, L. D. Brekke, T. Das, H. C. Hartmann, H. G. Hidalgo, M. Hoerling, and G. J. McCabe (2014), Understanding uncertainties in future Colorado River streamflow, *Bulletin of the American Meteorological Society*, *95*(1), 59-78.

West, A. J., and K. R. Knoerr (1959), Water losses in the Sierra Nevada, *Journal (American Water Works Association)*, *51*(4), 481-488.

Williams, M. W., and J. M. Melack (1991), Solute chemistry of snowmelt and runoff in an alpine basin, Sierra Nevada, *Water resources research*, *27*(7), 1575-1588.

Winchell, T. S., D. M. Barnard, R. K. Monson, S. P. Burns, and N. P. Molotch (2016), Earlier snowmelt reduces atmospheric carbon uptake in midlatitude subalpine forests, *Geophysical Research Letters*, *43*(15), 8160-8168.

The Cryosphere Discuss., https://doi.org/10.5194/tc-2017-123
Manuscript under review for journal The Cryosphere
Discussion started: 18 July 2017

Tables

Table 1. Meteorological station and snow measurement details. Station numbers are ranked by station elevation and correspond to those mapped in Fig. 1. The variables measured at each location are listed: air temperature (Ta), relative humidity (RH), wind speed (ws), precipitation (ppt), snow water equivalent (SWE), and snow depth (depth).

#	Station name	Elev., m	Measured variables*	Operating agency
Automated met. stations				
1	D0117	263	Ta, RH, ws	APRSWXNET
2	C4177	378	Ta, RH, ws	APRSWXNET
3	Ash Mountain	527	Ta, RH, ws, ppt	NPS
4	Shadequarter	1323	Ta, RH, ws	CDF
5	Wolverton	1598	Ta, RH, ws	NPS
6	Lower Kaweah	1926	Ta, RH, ws, ppt	NPS
7	Atwell	1951	ppt	USACE
8	Case Mountain	1967	Ta, RH, ws	BLM
9	Giant Forest	2027	Ta, ppt	USACE
10	Bear Trap Meadow	2073	ppt	USACE
11	Wolverton Meadow	2229	Ta, RH, ws	SNRI
12	Park Ridge	2299	Ta, RH, ws	NPS
13	Hockett Meadows	2592	ppt	USACE
14	Marble Fork	2626	Ta	ERI
15	Panther Meadow	2640	Ta, RH, ws	SNRI
16	Emerald Lake	2835	Ta, RH, ws	ERI
17	Farewell Gap	2896	Ta	USACE
18	Topaz Lake	3232	Ta, RH, ws, SW, LW	ERI
19	M3	3288	Ta, RH, ws	ERI
Automated snow stations				
1	Giant Forest	1951	SWE	USACE
2	Big Meadows	2317	SWE	USACE
3	Farewell Gap	2896	SWE, depth	USACE
Monthly snow courses				
1	Giant Forest	1951	SWE, depth	NPS
2	Big Meadows	2317	SWE, depth	CADWP
3	Mineral King	2439	SWE, depth	NPS
4	Hockett Meadow	2592	SWE, depth	NPS
5	Panther Meadow	2622	SWE, depth	NPS
6	Rowell Meadow	2698	SWE, depth	KRWA
7	Scenic Meadow	2942	SWE, depth	KRWA

*Meteorological variables used in this study.
APRSWXNET: Automatic Position Reporting System as a Weather NETwork
NPS: National Park Service (Sequoia and Kings Canyon National Parks)
CDF: California Department of Forestry
USACE: United States Army Corps of Engineers
BLM: Bureau of Land Management
SNRI: Sierra Nevada Research Institute, University of California Merced
ERI: Earth Research Institute, University of California Santa Barbara
CADWP: California Department of Water and Power
KRWA: Kaweah River Water Association

The Cryosphere Discuss., https://doi.org/10.5194/tc-2017-123
Manuscript under review for journal The Cryosphere
Discussion started: 18 July 2017

874 Table 2. Average (hourly) air temperature and shortwave radiation values measured at the alpine
875 Topaz Lake meteorological station in the Tokopah Basin for JFM and AMJ of the moderately
876 dry year (2009), near-average year (2008) and moderately wet year (2010).

	Air temperature, °C		Shortwave, W m^{-2}	
	JFM	AMJ	JFM	AMJ
2009	-3.2	3.3	163	279
2008	-3.6	3.4	166	317
2010	-4.0	1.3	152	306

877

The Cryosphere Discuss., https://doi.org/10.5194/tc-2017-123
Manuscript under review for journal The Cryosphere
Discussion started: 18 July 2017

878 Table 3. Mean daily values of hourly measured meteorological variables (nominal mean) during
879 the three mid-winter melt events in 2009 (see Fig. 10) compared to the average conditions
880 measured at eight stations > 2250 m asl computed on 11-days centered on the event dates,
881 averaged over the three years of the study. Precipitation is reported as the daily sum of measured
882 values. Melt rates simulated in the nominal case are reported as the mean value computed over
883 all grid elements > 2250 m asl and the maximum value over the full domain with the
884 corresponding elevation.
885

Met. variable	Jan. 21	Feb. 22	Mar. 1
Air temp., °C	2.8 / -0.5	-0.7 / 0.6	4.4 / 1.0
Shortwave, W m^{-2}	57 / 96	83 / 152	163 / 176
Longwave, W m^{-2}	292 / 232	297 / 226	266 / 217
Wind, m s^{-1}	4.0 / 4.3	4.6 / 4.0	7.2 / 4.4
Precipitation, mm	0.0	4.3	0.0
Mean melt rate, mm d^{-1} nom. sim. (>2250 m)	6.5	1.5	4.7
Max. melt rate, mm d^{-1} nom. sim. (elev., m)	30.6 (1897)	28.3 (1586)	44.0 (1741)

886

The Cryosphere Discuss., https://doi.org/10.5194/tc-2017-123
Manuscript under review for journal The Cryosphere
Discussion started: 18 July 2017

887 **Figures**

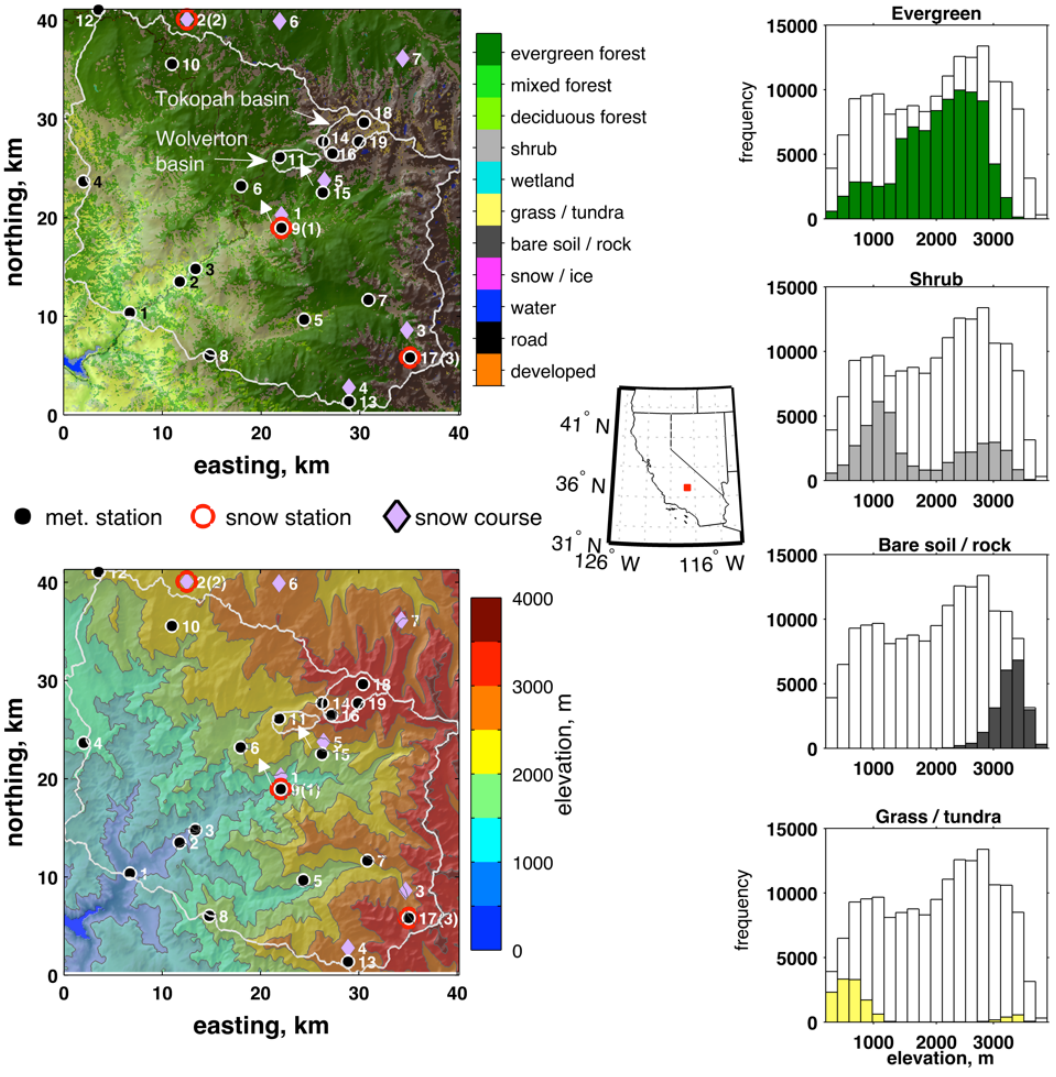

888

889 Figure 1: The elevation and land cover distribution of the model domain encompassing the
890 Kaweah River basin (outlined) on the western side of the southern Sierra Nevada, California.
891 Locations of the forested Wolverton and largely alpine Tokopah research basins are indicated.
892 The locations of 19 automated meteorological stations (filled circle markers), three automated
893 snow stations (red circles), and, seven monthly snow survey transects (diamond markers) are
894 shown. Station numbers, ranked by elevation, correspond to those in Table 1. The histograms
895 illustrate the elevation distribution of the four primary land cover types (colored bars) relative to
896 the elevation of the model domain (empty bars).

The Cryosphere Discuss., https://doi.org/10.5194/tc-2017-123
Manuscript under review for journal The Cryosphere
Discussion started: 18 July 2017

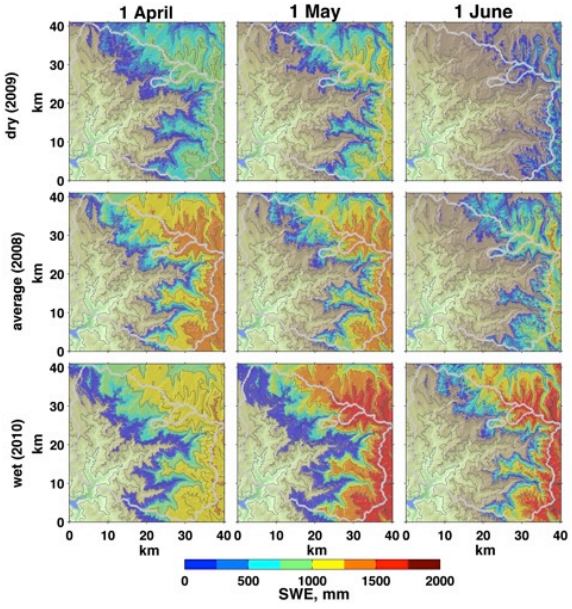

Figure 2: Simulated SWE over the greater Kaweah River basin on the first of April (left panel column), May (center panel column), and June (right panel column) for a moderately dry water year (2009; top panel row), near-climatological-average water year (2008; middle panel row), and a moderately wet water year (2010; bottom panel row).

The Cryosphere Discuss., https://doi.org/10.5194/tc-2017-123
Manuscript under review for journal The Cryosphere
Discussion started: 18 July 2017

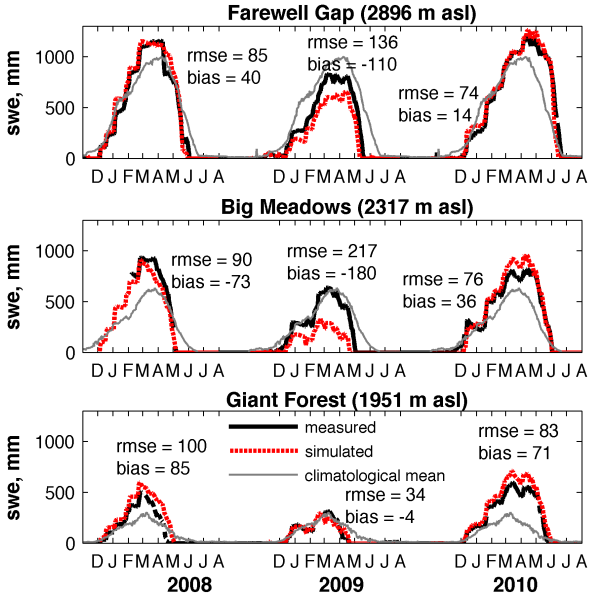

Figure 3: Measured and simulated SWE at the three automated snow stations spanning the middle elevations of the greater Kaweah River basin. The error metrics RMSE and bias, in millimeters, are provided for each station-year. The thin gray line indicates the long-term climatological mean SWE based on 26-years of data (1988 – 2014) collected at the Giant Forest and Big Meadows stations and a 15-year record (2000 – 2014) at the Farewell Gap station.

The Cryosphere Discuss., https://doi.org/10.5194/tc-2017-123
Manuscript under review for journal The Cryosphere
Discussion started: 18 July 2017

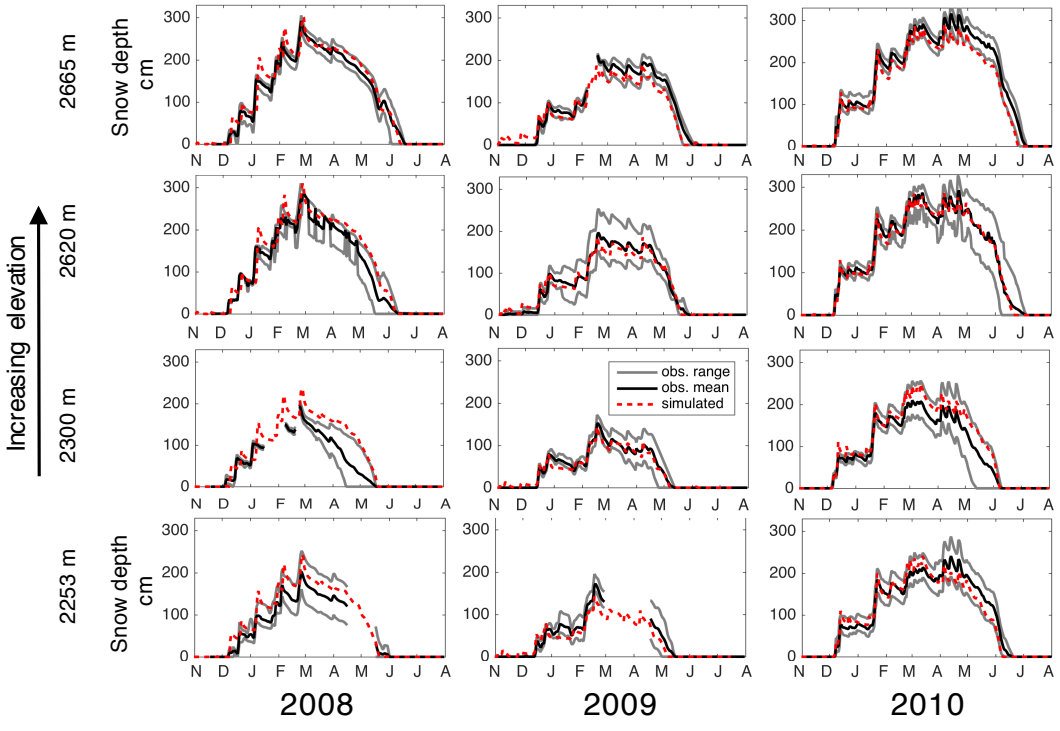

Figure 4: Comparison of three years (panel columns) of daily (x-axes) simulated (red lines) snow depth and the six-sensor observed range (gray lines) and mean (bold lines) snow depth measured by automated sensors at four research sites (panel rows) at different elevations in the Wolverton basin.

The Cryosphere Discuss., https://doi.org/10.5194/tc-2017-123
Manuscript under review for journal The Cryosphere
Discussion started: 18 July 2017

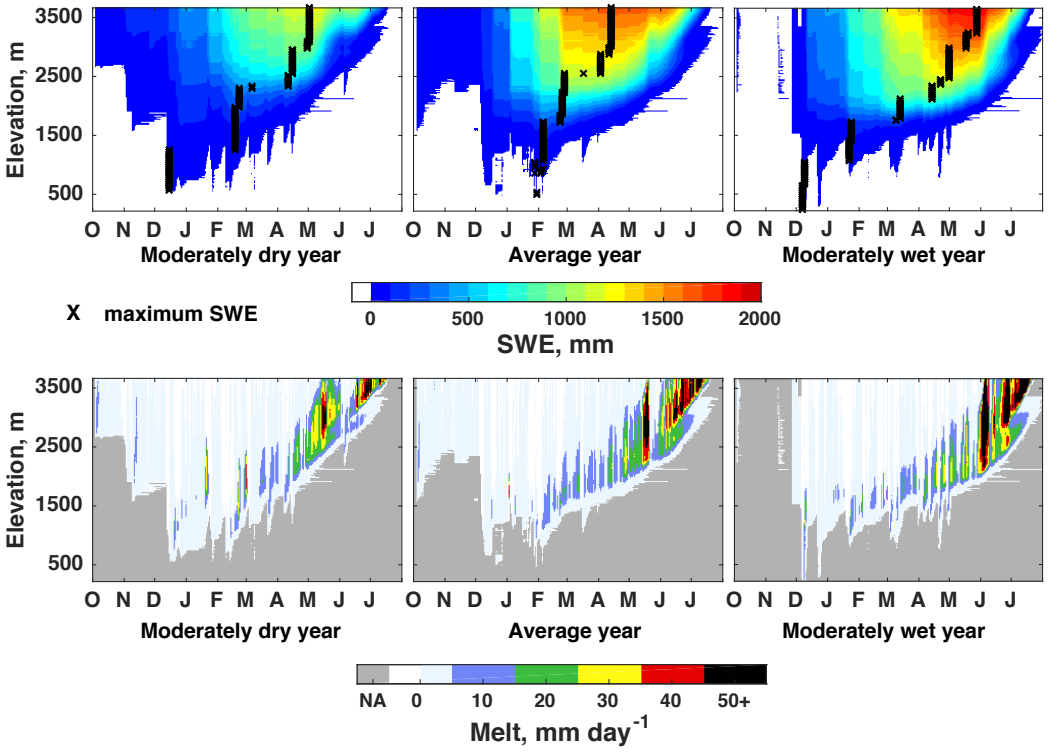

913
914 Figure 5: Distribution of (top panels) SWE and (bottom panels) daily melt by elevation (mean
915 values within 18 m elevation bins; y-axes) and time (daily; x-axes) for a moderately dry (2009;
916 left column panels), near-average (2008; center column panels), and moderately wet (2010; right
917 column panels) snow season. The grey color in the lower panels indicates times when there is no
918 snow to melt (NA). The elevation-specific dates of maximum SWE are indicated.

The Cryosphere Discuss., https://doi.org/10.5194/tc-2017-123
Manuscript under review for journal The Cryosphere
Discussion started: 18 July 2017

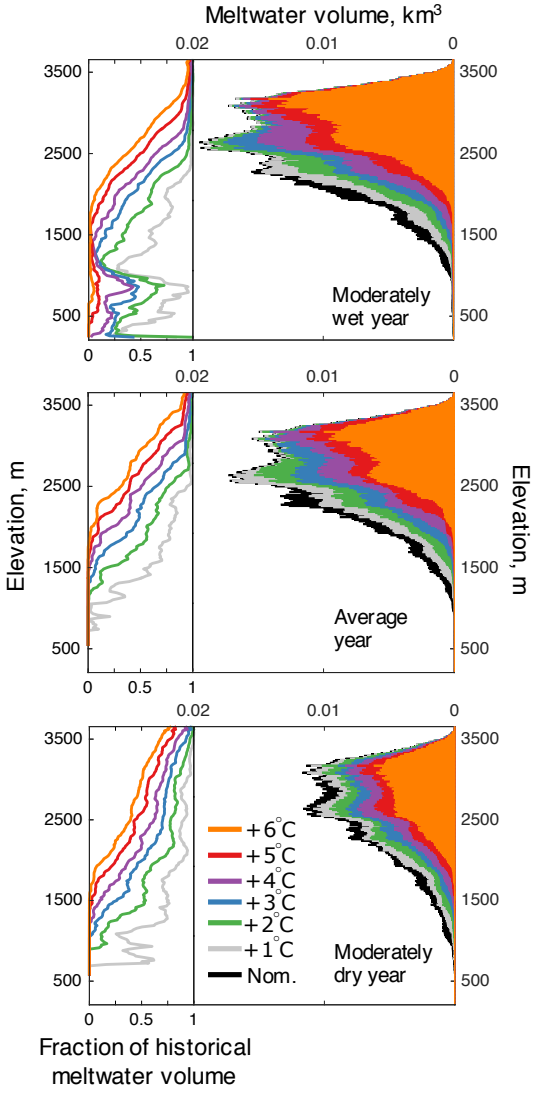

Figure 6: The elevation distribution (y-axes) of (right bar graphs) simulated annual meltwater volume and (line graphs) the fraction of that historical meltwater for each warmer scenario (colors; see legend) for the (top) moderately wet, (middle) average, and (bottom) moderately dry snow seasons. The total meltwater was summed within the same elevation bins used in Fig. 5.

The Cryosphere Discuss., https://doi.org/10.5194/tc-2017-123
Manuscript under review for journal The Cryosphere
Discussion started: 18 July 2017

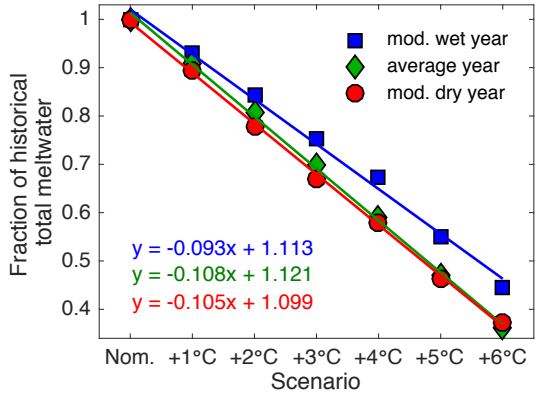

Figure 7: The fraction of simulated domain-wide historical meltwater (y-axis), relative to the nominal case, for each warmer temperature scenario (x-axis) for the three years (marker type and color). The colored lines and associated regression equations show linear fits to the data. For each year, the R^2 value was > 0.99 and the p-value was ≪ 1e-6.

The Cryosphere Discuss., https://doi.org/10.5194/tc-2017-123
Manuscript under review for journal The Cryosphere
Discussion started: 18 July 2017

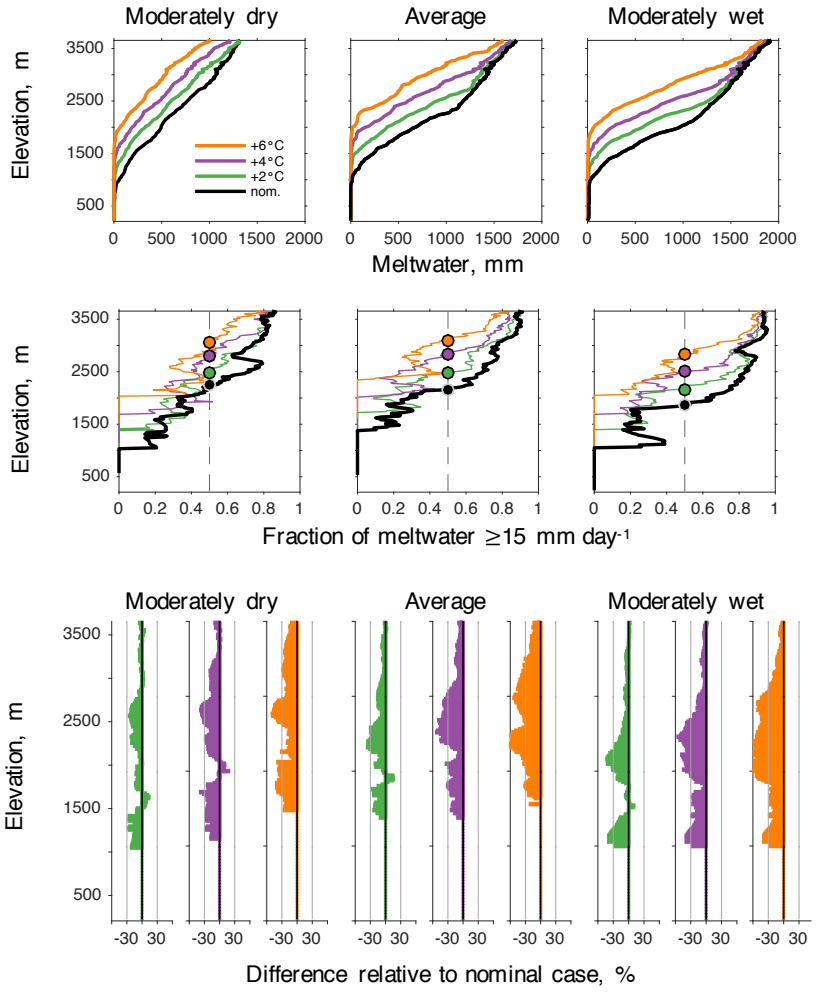

Figure 8: The elevation distribution (y-axes) of (top row of panels) the average total depth of annual meltwater (x-axes) simulated for the nominal case (black lines) and select perturbed temperature scenarios (colored lines), and (second row of panels) the fraction of annual meltwater produced at snowmelt rates ≥15 mm day^{-1}. The colored circles indicate elevations at which simulated melt occurs equally at rates ≥15 mm day^{-1} and <15 mm day^{-1}. The lower panels of colored graphs show the differences from the nominal case, reported in percent of annual meltwater, produced at snowmelt rates ≥15 mm day^{-1} for the three select scenarios. Results are shown for the moderately dry (2009; left column of plots), near-average (2008; middle column of plots), and moderately wet (2010; right column of plots) snow seasons.

The Cryosphere Discuss., https://doi.org/10.5194/tc-2017-123
Manuscript under review for journal The Cryosphere
Discussion started: 18 July 2017

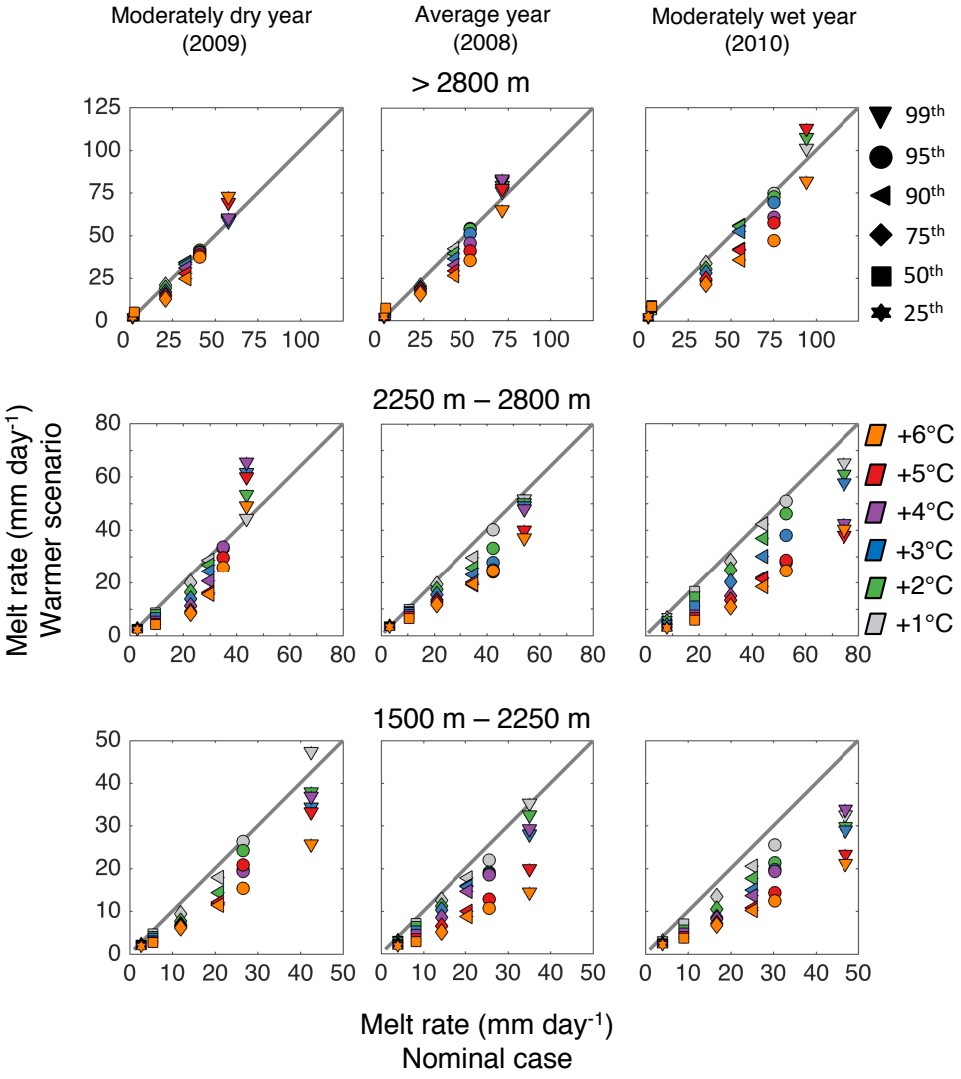

Figure 9: Quantile plots of simulated melt rates for the nominal (x-axes) and warmer scenarios (y-axes) for model grid cells characterized as high elevation (> 2800 m; top row of panels), middle elevation (2250 m – 2800 m; middle row of panels) and lower elevation (1500 m – 2250 m) regions for the moderately dry year (left column), average year (middle column) and moderately wet year (right column). Marker colors correspond to the six different temperature perturbations. Plotted in each graph are the 25th, 50th, 75th, 90th, 95th, and 99th percentiles (marker shapes) of daily snowmelt rates ≥ 1 mm day^{-1} for all grid cells within each water year and elevation range. The 1:1 lines are plotted for reference.

The Cryosphere Discuss., https://doi.org/10.5194/tc-2017-123
Manuscript under review for journal The Cryosphere
Discussion started: 18 July 2017

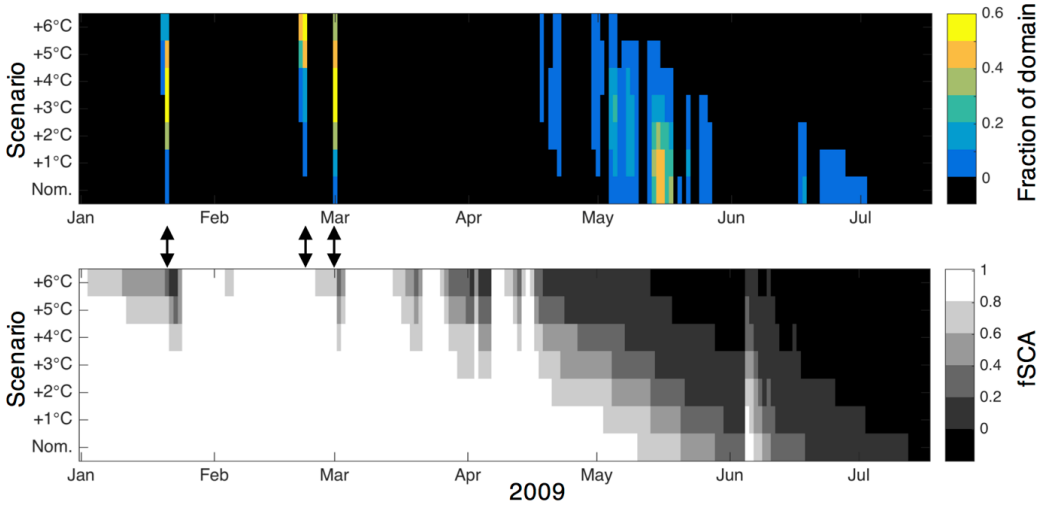

Figure 10: Daily extreme snowmelt in 2009 (melt rates > 40 mm day^{-1} at model grid cells > 2250 m asl, corresponding to extreme melt rates [≥ 99th percentile]; see Fig. 8) as simulated by the nominal (Nom.) and six perturbed temperature scenarios (y-axes) shown as the (top panel) fraction of the area undergoing extreme melt. The lower panel shows the fraction of snow-covered area (fSCA) for the same time period and domain. Arrows indicate (winter) melt events (see Table 3 for meteorological conditions and averages).